ACS Catalysis

Research Article

pubs.acs.org/acscatalysis

In Situ Transformation of Hydrogen-Evolving CoP Nanoparticles: Toward Efficient Oxygen Evolution Catalysts Bearing Dispersed Morphologies with Co-oxo/hydroxo Molecular Units

Jaeyune Ryu,[†] Namgee Jung,[†,§] Jong Hyun Jang,[†] Hyoung-Juhn Kim,[†] and Sung Jong Yoo*[,†,‡]

[†]Fuel Cell Research Center, Korea Institute of Science and Technology (KIST), Seoul 136-791, Republic of Korea

[‡]Department of Clean Energy and Chemical Engineering, Korea University of Science and Technology, Daejeon 305-350, Republic of Korea

Supporting Information

ABSTRACT: Reported herein is elucidation of a novel Co-based oxygen evolution catalyst generated in situ from cobalt phosphide (CoP) nanoparticles. The present CoP nanoparticles, efficient alkaline hydrogen-evolving materials at the cathode, are revealed to experience unique metamorphosis upon anodic potential cycling in an alkaline electrolyte, engendering efficient and robust catalytic environments toward the oxygen evolution reaction (OER). Our extensive ex situ characterization shows that the transformed catalyst bears porous and nanoweb-like dispersed morphologies along with unique microscopic environments mainly consisting of discrete cobalt-oxo/hydroxo molecular units within a phosphate-enriched amorphous network. Outstanding OER efficiency is achievable with the activated catalyst, which is favorably comparable to even a precious iridium catalyst. A more remarkable feature is its outstanding long-term stability, superior to iridium and conventional cobalt oxide-based materials. Twelve-hour bulk electrolysis continuously operating at high current density is completely tolerable with the present catalyst.

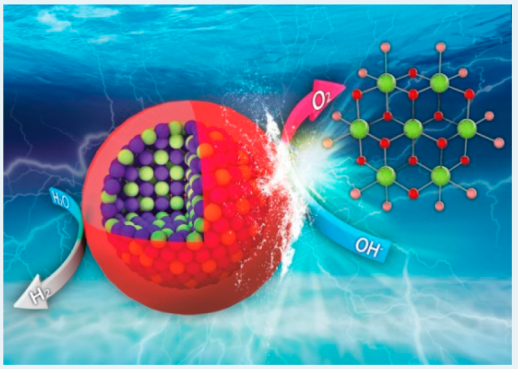

KEYWORDS: *water splitting, oxygen evolution, hydrogen evolution, cobalt phosphide nanoparticle, in situ transformation*

1. INTRODUCTION

Converting water to O_2 and H_2 has been regarded as a central chemistry of energy conversion technologies for the storage of renewable sources in the form of chemical fuels. Indeed, water splitting can be a highly economical way for providing a sustainable source of hydrogen to many renewable-energy technologies.[1]

Water−alkali electrolysis can be viewed as a combination of two half-cell reactions—the hydrogen evolution reaction (HER, $2H_2O + 2e^- \rightarrow H_2 + 2OH^-$) and the oxygen evolution reaction (OER, $4OH^- \rightarrow O_2 + 2H_2O + 4e^-$)—that occur at the cathode and anode, respectively. In practice, however, large-scale electrochemical production of hydrogen from water splitting is hampered by a lack of stability of electrode materials and high overpotentials of HER and OER in alkaline solutions. Particularly, a key drawback to making water splitting viable on industrial level is the inefficiency of available electrocatalysts for the oxygen evolution reaction (OER), which is a far more complex process than the hydrogen evolution reaction (HER). OER is the most energy-intensive step in the overall electrolysis process because of the sluggish kinetics associated with O−H bond breaking and attendant O═O bond formation as well as the need to perform proton-coupled electron transfer chemistry at the high equivalency of 4.[1,2] Although precious metal oxide catalysts such as RuO_2 and IrO_2 exhibit high OER activities,[3] their large-scale applications are impeded by their prohibitive cost, scarcity, and poor stability in long-term operation in alkaline media. Therefore, developing effective and robust OER catalysts from earth-abundant elements to substitute the high cost catalysts is highly demanding.

Among nonprecious metals for alkaline OER catalysis, cobalt has drawn remarkable attention. Various cobalt oxide-based materials, including nanostructured Co_3O_4, Co_3O_4-based hybrids, and substituted cobaltites ($M_xCo_{3-x}O_4$), have been ardently designed.[4] Without M_4O_4 topology, Co-based perovskites,[5a] cobalt aluminophosphate,[5b] $Mn_3O_4/CoSe_2$,[5c] Co−Mn−Ga spinel oxides,[5d] Zn−Co layered double hydroxide,[5e] $CoSe_2$ nanosheets,[5f] and $CeO_2/CoSe_2$ nanobelts[5g] have been revealed as active alkaline systems. More recently, introduction of supportive materials has been pursued for enhancing the catalytic efficiency of the cobalt center. In addition to gold,[6] carbon-based materials have attracted much interest.[7] Coupling N-doped graphene or carbon nanotubes

Received: February 17, 2015
Revised: May 7, 2015
Published: May 21, 2015

© 2015 American Chemical Society

DOI: 10.1021/acscatal.5b00349
ACS Catal. 2015, 5, 4066−4074

with cobalt oxide nanoparticles could synergistically enhance the OER efficiency and even durability in an alkaline solution.[7]

Previous catalyst research has focused mainly on the elucidation of desirable composites for the as-prepared state of nanomaterials. As the potential is raised to the onset of OER, however, catalyst materials will be progressively transformed. The extent of change and overall redox switching behaviors exhibited by each of the metals and metal oxides in contact with an aqueous solution are not fully understood.[8,9] In this sense, understanding and controlling the restructuring behavior of the materials under anodic conditions should be a focus of catalyst development because the transformed state closely defines the catalyst's steady-state performances.[9]

In general, catalyst functionality strongly relies on microscopic local structures. Such microscopic environments of the catalyst have a close relationship with its macroscopic properties, such as dispersity, porosity, and amorphosity, which often determine the density of the internal active sites.[8] At the outset of the present work, we noticed that ligand species are essential components in several oxygen-evolving complexes (OEC) that take advantage of a high density of active sites by incorporating molecular cluster structures as active domains. Particularly in nature, Mn_3CaO_4 cores of the OEC in photosystem II are systemically ligated by carboxylates in amino acid residues (Figure 1a), which are revealed to be

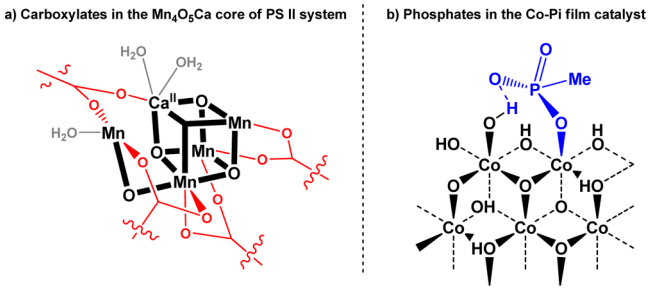

Figure 1. Examples of ligand systems for the active molecular domains in serveral OECs.

required for proper assembly and function of the OEC.[10] As the effective homogeneous OECs and structural analogies to the Mn_3CaO_4 core, molecular Co_4O_4 cubanes[11] and polyoxometallate-stabilized Co oxide clusters[12] have been synthesized with a proper use of ligands. Significant roles of the ligand are also highlighted in heterogeneous catalysts. In an amorphous cobalt−oxide−phosphate (Co−Pi) film catalyst, prepared through in situ electrodeposition of Co (II) ions in phosphate buffer,[13] phosphate controls the self-assembly of the catalytic structures, providing unique local environments consisting of active molecular crystallites in an amorphous network (Figure 1b).

Inspired by the above-mentioned aspects, we envisioned development of a novel oxygen evolution catalyst by employing unique reassembling behavior of a modified Co-based nanoparticle system. We expected that possible ligating species within the precursive nanoparticle would control redox-swiching properties and the restructuing nature of the material upon anodic potentials to induce desirable catalytic environments. Described herein is the discovery of a new oxygen-evolving catalyst generated in situ from cobalt phosphide (CoP) nanoparticles. We found that the present CoP nanoparticles experience dramatic metamorphosis under anodic potentials, engendering nanoweb-like dispersed morphologies and unique microscopic local structures that have rarely been avaiable with other Co-based nanoparticle systems. Not only excellent OER efficiency comparable to a precious iridium catalyst, but also remarkable durability was achieved by the activated catalyst. Our findings would reap more benefits when considering the fact that preparation of the present percursive CoP system is easily available. On the other hand, original as-prepared CoP nanoparticles display highly efficient and durable alkaline hydrogen-evolving properties at cathodic potentials, even comparable to the best precious Pt/C catalyst. Along with those versatile natures of the present CoP nanoparticles depending upon the applied potentials, we present efficient alkaline electrocatalyst systems for both HER and OER from one material (Figures 2, S1).

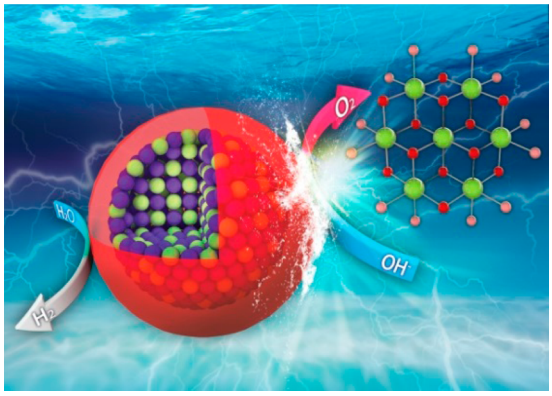

Figure 2. In situ reassembly of hydrogen-evolving CoP nanoparticles toward unique and effective OEC.

2. RESULTS AND DISCUSSION

2.1. Preparation of CoP Nanoparticles and Characterization. On the basis of our modified synthetic methods using trioctylphosphine (TOP) as a P source,[14a−c] a CoP nanoparticle−carbon black hybrid material was synthesized in one pot through thermal decomposition of cobalt complexes in a solution containing Vulcan XC-72 (see the Supporting Information for details). Pregenerated Co-TOP complex was added dropwise to a carbon suspension containing oleylamine at 300 °C, where the further reaction between Co monomers[14d] (presumed reactive intermediates), and TOP was promptly facilitated. After the reaction finished, a washing process and heat treatment (360 °C, 1 h) under argon atmosphere were conducted to remove chemical residues. The resultant hybrid material (hereafter denoted as CoP/C) contained rod-shaped CoP nanoparticles (~20 nm) on carbon support with ~13 wt % of cobalt and ~8 wt % of phosphorus (Figures 3, S2).

X-ray diffraction (XRD) peaks matched with orthorhombic cobalt phosphide (CoP, JCPDS-29−0497) signify a majority phase of CoP composite (Figure S3).[14] In addition, its (111), (112), and (211) planes can be identified through high-resolution transmission electron microscope (TEM), by referring to the distance between adjacent planes and selected area electron diffraction patterns (Figure S4). In addition, it was observed that crystalline ranges of CoP nanoparticles are surrounded by thick amorphous-like shells (~5 nm), composed of {Co, P, O} (Figure 3). According to the energy dispersive X-ray spectroscopy (EDS) analysis, the shells were revealed to

DOI: 10.1021/acscatal.5b00349
ACS Catal. 2015, 5, 4066−4074

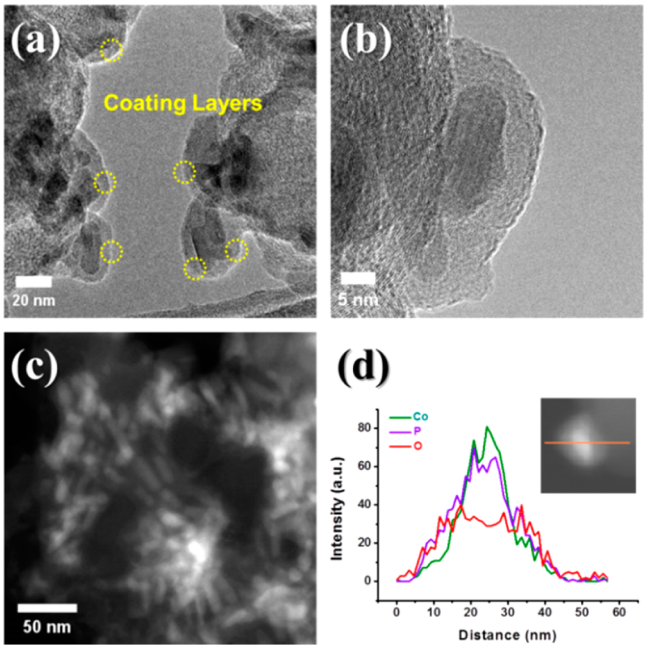

Figure 3. (a, b) TEM images and (c) STEM image of as-prepared CoP/C. (d) EDS line profiling spectra of a CoP nanoparticle (inset: a STEM image of the CoP nanoparticle marked with a profile path).

have higher P contents compared with the core side of the nanoparticles (Figures 3d, S5). Such amorphous outer layers were found in other metal phosphide nanoparticles.[14b,15]

We further investigated the surface of the as-prepared CoP nanoparticles through X-ray photon spectroscopy (XPS) and X-ray absorption near edgy spectroscopy (XANES) (Figure S6). The position of the main peaks (~783 eV) with broad shoulder features (~785−790 eV) in the Co $2p_{3/2}$ XPS spectrum clearly indicates the presence of Co^{II} species bound to oxygen[16] while the contribution of the reduced state cobalt(0) (~779 eV) is negligible. The p_{2p} region of CoP/C also displays a dominant signal of oxidized phosphorus species (~135 eV, PO_3^-, metaphosphate[5h,16d,17]) rather than that of phosphides (~129−130 eV) (Figure S6).[18,19] Most of the obtained XPS signals probably correspond to its ~5 nm thick amorphous layers we have already described, and we believe that is the reason why signals for the reduced state of cobalt phosphide (core side) are weakly detected (Figure S7). In addition, the edge position of CoP/C in XANES (7725 eV, Figure S6) represents the richness of the Co species with an average valency of 2,[13f] which is very consistent with the XPS result. All results enable us to tentatively describe the surface of the CoP nanoparticles as an amorphous-like mixture of Co metaphosphate and cobalt oxo/hydroxo species, mostly in a 2+ state. In fact, those aspects are quite consistent with previous reports that metal (Ni or Co) phosphides have a larger sensitivity to air, eventually bearing higher amounts of metal oxides and oxidized phosphorus species at the surface.[19]

2.2. Anodic Behaviors of CoP Nanoparticles: In Situ Transformation toward OER Catalyst. With enough information about the electronic and structural nature of the present CoP nanoparticles, we next investigated its redox switching behaviors upon potential cycling that covers the OER region. Figure 4a displays the first and second scans of cyclic voltametry (CV) for the present CoP/C, measured in 0.1 M KOH solution (pH 13). The first oxidative sweep of the CoP/C produced prominent anodic currents with a huge preoxidation peak over the broad potential range prior to the onset of OER (~1.5 V). The highly extensive oxidative currents compared with the corresponding reverse reductive currents imply that irreversible oxidative transformation of CoP occurs during the first scan (Figure S8). On the basis of the general electrochemical redox states of cobalt upon potential bias,[8,20] it is speculated that Co^{II} species at the surface of CoP are oxidized to higher valent states (≥3+) during the transformation. Stabilized steady-state currents over the whole range (including the OER region) are just obtained from the second scan, at which the preoxidation peak was significantly diminished and shifted toward ~1.1 V (Figure S8). In addition, overall oxidative and reductive currents became almost reversible at the steady state. Of note, a catalyst activation phenomenon was also detected in the polarization curves and its tafel plots at the OER region (Figure 4b). Not only is the onset potential measured in the second scan ~20 mV smaller than the first scan, but also the tafel slope obtained from the second scan exhibits a distinctively smaller value (66 mV dec^{-1}) than that of the first scan (83 mV dec^{-1}). Decreasing the tafel slope and onset potential indicate improving OER kinetics during the initial potential cycling. Clearly, steady-state OER performance will be defined by the transformed nature of the present CoP.

Significant macroscopic transition of the nanoparticle was accompanied by the electrochemical catalyst activation (Figures 4c, S9, and S10). As revealed in a scanning transmission electron microscope (STEM) image (Figure 4c), the original rod-shaped CoP nanoparticles were changed into porous and nanoweb-like dispersed architectures, even after just one CV cycle (1.0−1.8 V, 5 mV s^{-1}). Although EDS-mapping confirms colocation of Co, P, and O elements within the transformed nanostructure (Figures 4d, S11), reduced P/Co ratio indicates that some P species were leached out during the transformation (Figure S10). Meanwhile, potential cycling with a reduced upper limit (1.0−1.5 V, the range corresponds to where the prominent preoxidative currents are recorded) induced a similar level of dispersed morphology (Figure S12); therefore, the substantial morphology transition is believed to proceed through an oxidative manner in advance of the onset of oxygen evolution.

To elucidate microscopic local structures of the activated catalyst, ex situ X-ray analysis was conducted (Figure 5a−c, red lines). The activated catalyst was recovered after the potential cycling over the OER region (1.0−1.8 V, 5 mV s^{-1}, 2 cycles) and subsequently analyzed. First, in Co $2p_{2/3}$ XPS, the activated post-OER state exhibits a shift of the main peak (~1 eV) along with diminished shoulder features compared with the original state, indicating a transition of the original Co^{II} species to higher oxidation states during the catalyst reassembly (Figure S6).[5h,16] A positive shift of edge energy in XANES also suggests increasing oxidation states of cobalt after metamorphosis (Figure 5a). The edge for the activated catalyst is ~5 eV higher in energy (7730 eV) than that of the as-prepared state, thus being consistent with an average Co valency of ≥III.[13f] This change matches well with the already-discussed CV data (Figure 4a) in which irreversible oxidation of Co^{II} species are recorded. In addition, a change in the P state was evident: a noticeable shift of the P 2p peak is ascribed to the transition of the initial P−O species (metaphosphate) into phosphate groups (~134 eV, PO_4^{2-}) (Figure 5b).[5h,13a,c] Our additional fitting analysis ensured the presence of phosphate species in the activated catalyst (Figure S7),[13c] and a P/Co ratio measured

DOI: 10.1021/acscatal.5b00349
ACS Catal. 2015, 5, 4066−4074

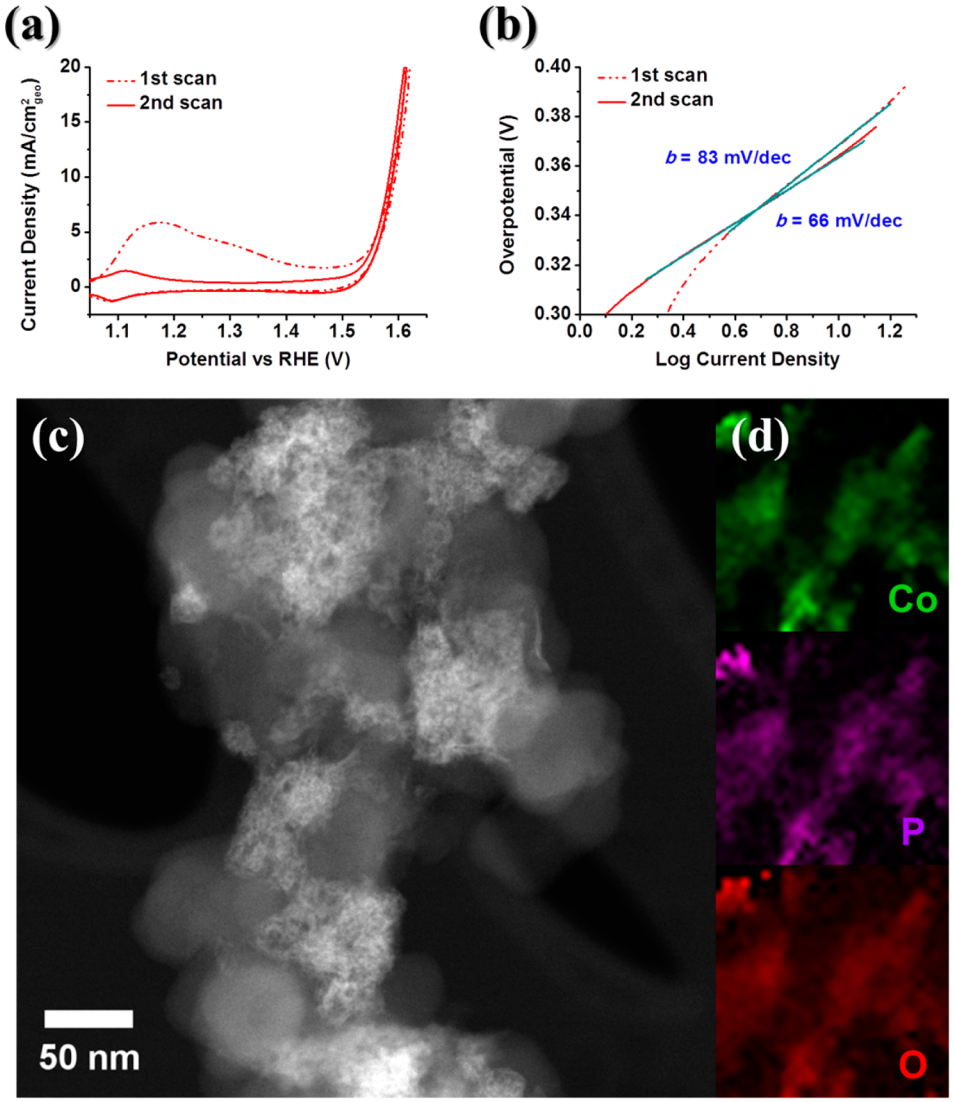

Figure 4. (a) CV scans (*iR*-compensated) and (b) tafel plots of CoP/C measured in 0.1 M KOH with a sweep rate of 5 mV s^{-1} (catalyst loading: 0.05 mg_{Co} cm^{-2}). (c, d) STEM and EDS mapping images of CoP/C after potential cycling.

higher in XPS than in EDS (Figures S10, S13) demonstrates the relatively outer position of phosphates in the transformed nanostructure. According to the XPS analysis for the carbon states (Figure S14), on the other hand, peak features from the oxygen-bound carbon and sp^3 carbon species (291−287 eV) are reduced during OER catalysis, which might indicate the conductivity enhancement of the carbon components.[21]

The transition of the extended X-ray absorption fine structure (EXAFS) of CoP proves its evolution of local structures during catalyst activation (Figure 5c). Compared with CoO, Co_3O_4 (Figure 5e,f), and CoO(OH) crystalline phases,[13f] distinctive EXAFS patterns for the activated state of CoP represent its unique microscopic environments. Of note, it is quite remarkable that XANES and Fourier-transformed EXAFS features of the activated ex situ state of CoP bear great resemblance to those of the catalytic turnover state of the Co-Pi catalyst.[13f] Several independent EXAFS investigations of the Co-Pi catalyst agree on the presence of molecular-sized ordered crystallites in an amorphous network;[13e−g] however, two different arrangements of the CoO_6 molecular units, both compatible with the experimental EXAFS spectra, have been proposed: either clusters of complete and incomplete vertex-sharing cobalt-oxo cubane motifs[13e] or layered edge-sharing CoO_6 octahedra (Figure 5d).[13f] In fact, the latter edge-sharing molecular unit is the basic structural component of the extended planes of the CoO(OH); therefore, they share some major features in EXAFS but with clear differences.[13f]

According to the widely accepted EXAFS analysis for the Co-Pi catalyst,[13f,g] the indicated peaks I and II in the EXAFS spectrum of the activated CoP correspond to the nearest-neighbor Co−O and Co−Co vectors, respectively (Figure 5c). Their locations and relative intensity ratio (I > II) as well as lack of intense peaks at higher R' values (region III) that result from the long-range scattering interactions are well fit to the molecular nature of both Co-oxo/hydroxo clusters as depicted in Figure 5d. On the basis of these results, we expect that the local structure of the activated CoP is composed mainly of bis-oxo/hydroxo-bridged Co ions in discrete molecular units arranged into a phosphate-enriched amorphous network. Retention of such a discrete molecular nature in the ex situ steady state might be ascribed to the unique stabilizing effects of phosphate in the local structures. Of note, the EXAFS features of the activated CoP are in contrast with those of the CoO(OH) phase, which exhibits a bulk crystalline nature: a

DOI: 10.1021/acscatal.5b00349
ACS Catal. 2015, 5, 4066−4074

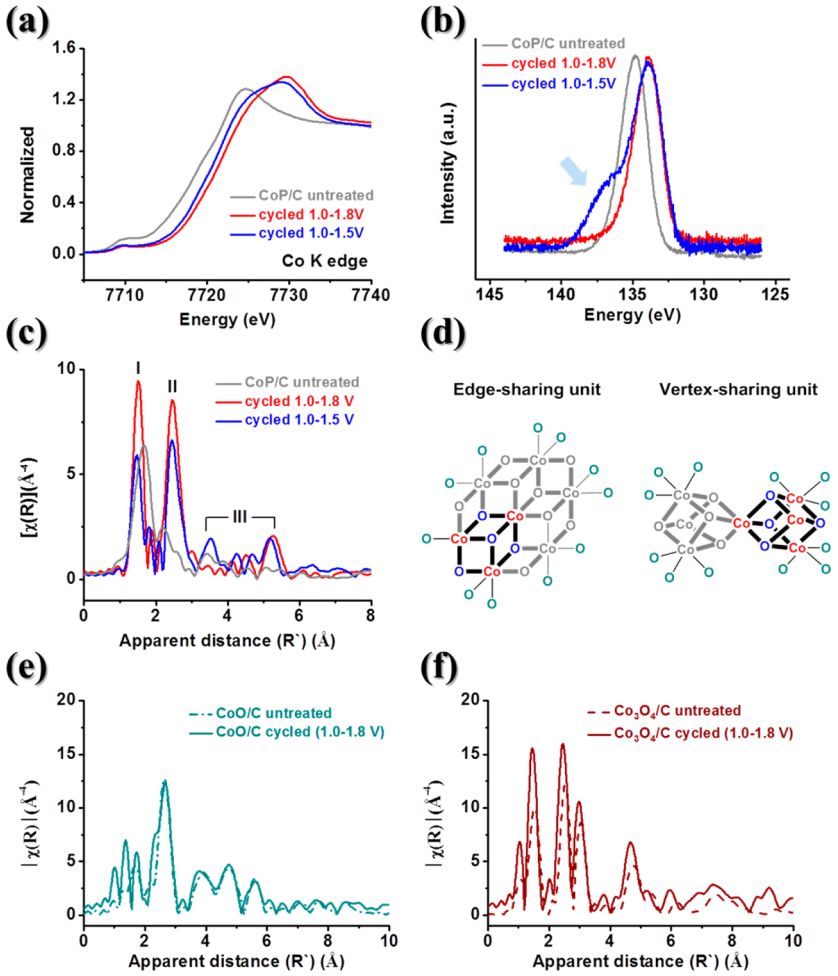

Figure 5. (a) XANES profiles, (b) P 2p XPS spectra, and (c) EXAFS spectra (Fourier transforms of *k*-space oscillations) of CoP/C before and after potential cycling. (d) Possible molecular structures represent the local environment of the present catalyst. Nonbridging oxygen ligands (phosphate, hydroxide, and water) are marked in green. (e, f) EXAFS spectra (Fourier transforms of *k*-space oscillations) of CoO/C and Co_3O_4/C before and after potential cycling.

greater intensity of the Co−Co vector than the Co−O vector (inverse to the activated CoP) along with more prominent features in region III.[13f]

To understand more about the transformative behavior and activation process of the present CoP nanoparticle in microscopic dimensions, we extended our ex situ X-ray analysis for the intermediate state gained from the reduced potential cycling (1.0−1.5 V) (Figure 5a−c, blue lines), which induced macroscopic features similar to those of the post-OER state (Figure S12). Although general EXAFS patterns (presence and locations of major peaks, I and II) are similar, noticeable differences were recorded on the spectrum along with an ∼2 eV lowered edge energy in XANES. Compared with the activated post-OER state, the intermediate state exhibits an inverse relative intensity between the major peaks (I < II) and more evident spectral features associated with longer Co−Co vectors (region III). Those characteristics are closely matched to the CoO(OH) phase, thus indicating the presence of bulkier crystallites composed of the Co-oxo/hydroxo edge-sharing structural motif in the intermediate state.[13f] Remarkably, another higher-valent P species in addition to the phosphate group was identified in the P 2p XPS spectrum of the intermediate state (Figure 5b), which might be possible evidence for a contribution of P ligands on the catalyst reassembly, presumably varying its coordination mode or chelating manner during the redox switching process of cobalt. To sum up, all those results suggest that the molecular nature in the local structures of activated CoP are "in situ"-generated beyond the onset of oxygen evolution (>1.5 V) associated with a kind of oxidative decomposition pathway under the influence of P species. Meanwhile, the negligible solubility of Co^{II} ions at 0.1 M KOH (pH 13) will disfavor the dissolution-/redeposition-based mechanism for catalyst reassembly.[9]

The unique anodic behavior of the present CoP nanoparticle, which contains a mixture of cobalt metaphosphate and cobalt oxo/hydroxo species, mostly in the 2+ state, is further emphasized when compared with other Co^{II}-rich nanoparticle systems. According to our ex situ analysis for comparison, both CoO and Co_3O_4 nanoparticles exhibit a negligible XANES edge shift (Figure S15) and minute EXAFS transition upon the identical potential cycling (Figure 5e,f). The exclusive molecular nature found in the ex situ state of CoP cannot be identified in that of CoO and Co_3O_4 nanoparticles. Consistently, anodic potential cycling in the region of oxygen evolution could not change their original compact nanostructures and crystalline bulk composites (Figure S16).[22] Only a limited surface region of the nanoparticles would be transformed under the application of external bias (according

DOI: 10.1021/acscatal.5b00349
ACS Catal. 2015, 5, 4066−4074

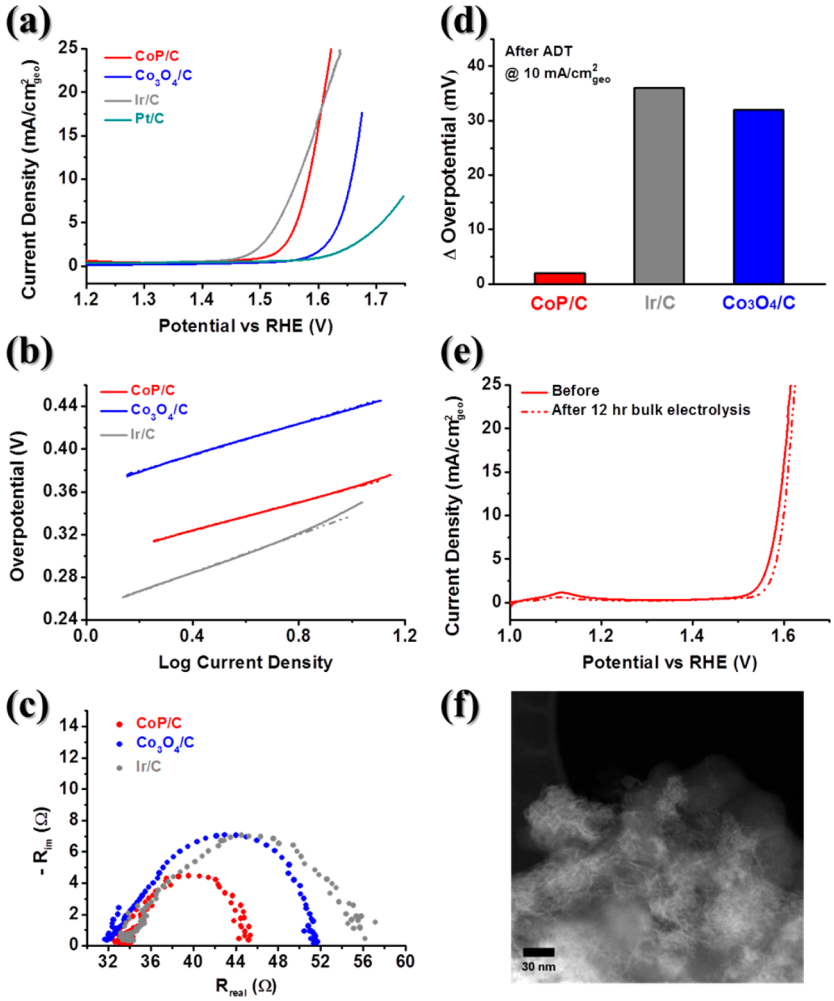

Figure 6. (a) OER polarization curves measured in 0.1 M KOH with a sweep rate of 5 mV s^{-1} (catalyst loadings: ~0.05 mg cm^{-2} for cobalt and ~0.08 mg/cm^2 for iridium and platinum). (b) Tafel plots of CoP/C (66 mV dec^{-1}), Co_3O_4/C (73 mV dec^{-1}), and Ir/C (89 mV dec^{-1}) extracted from part a. (c) EIS spectra of CoP/C, Co_3O_4/C, and Ir/C measured at 1.7 V. (d) Overpotential increase of CoP/C, Co_3O_4/C, and Ir/C at 10 mA/cm^2 after ADT test (1000 cycles, 1.3−1.7 V 100 mV s^{-1}). (e) OER polarization curves of CoP/C measured in 0.1 M KOH with a sweep rate of 5 mV s^{-1} before and after 12 h of bulk electrolysis continuously operating at a constant current density, 6 mA cm^{-2}. (f) STEM image of CoP/C after the 12 h of bulk electrolysis. All polarization curves in Figure 6 were *iR*-compensated (R ~ 30 ohm).

to previous in situ Raman study for cobalt oxide films and theoretical confirmation, bulk CoO(OH) phase has been suggested as a stable composite during catalytic turnover[6,23]). The present comparison clearly shows that the inherent nature of the CoP nanoparticle engendered by P incorporation elicits the induction of unique morphologies and molecular natures in local environments upon anodic potential cycling.

2.3. Steady-State OER Performances of the In Situ Transformed Catalyst. With enough understanding of the anodic behavior of the present CoP nanoparticles, we tried to assess the steady-state OER performances of the activated catalyst, which continues to be denoted as CoP/C for simplicity. Figure 6a shows OER polarization curves of the cobalt-based materials (CoP/C and Co_3O_4/C) and precious metal catalysts (Ir/C and Pt/C) deposited onto a glassy carbon working electrode at similar catalyst loadings, measured on a rotating disk electrode (RDE) in 0.1 M KOH solution (pH 13). With higher currents and an earlier onset of the catalytic current (Figure 5a), CoP/C displayed OER activities superior to those of Co_3O_4/C (~17 wt %) which contains cubic-shaped Co_3O_4 nanoparticles, the particle size (~15 nm size) of which is similar to that of the original CoP (Figure S16). A current density of 10 mA cm^{-2}, which is a frequently used standard metric in the OER literature and solar fuel synthesis,[24] was achievable at a small overpotential of 0.36 V with the CoP/C. Reproducibility of the catalytic activity was checked through repeated measurements (Figures S8, S17). Despite its low catalyst loading (~0.05 mg cm^{-2} for cobalt mass), the performance compares favorably with the best reported cobalt-based materials operating at base, including the recently revealed $Mn_3O_4/CoSe_2$ nanocomposite (0.2 mg/cm^2, overpotential of ~0.36 V, pH 13),[5c] Zn−Co-LDH (0.28 mg/cm^2, overpotential of ~0.5 V, pH 13),[5e] $CoSe_2$ nanosheets (0.14 mg/cm^2, overpotential of ~0.32 V, pH 13),[5f] $CeO_2/CoSe_2$ (0.2 mg/cm^2, overpotential of ~0.34 V, pH 13),[5g] Co_3O_4/N-graphene (0.2 mg/cm^2, overpotential of ~0.4 V, pH 14),[7a] and $CoSe_2$/N-graphene (0.2 mg/cm^2, overpotential of ~0.4 V, pH 13).[7d] Furthermore, the anodic current densities of CoP/C even approximate those of precious Ir/C. In addition, the tafel slope of CoP/C (66 mV dec^{-1}) is smaller than that of Co_3O_4/C (73 mV dec^{-1}) and Ir/C (89 mV dec^{-1}) (Figure 6b), which suggests that the oxygen evolution reaction mediated by CoP follows a kinetically more efficient pathway. According to electrochemical impedance spectroscopy (EIS) measurements

DOI: 10.1021/acscatal.5b00349
ACS Catal. 2015, 5, 4066−4074

(Figures 6c, S18), the activated catalyst exhibited the smallest charge transfer resistance at OER-occurring potential (1.7 V) as compared with that of Co_3O_4/C and Ir/C, implying its high feasibility in shuttling charges during catalytic turnover. Those benefits of activated CoP might be from its morphological advantages and unique molecular nature in the local environments.

The outstanding durability of CoP/C should be noted. The activated catalyst afforded negligible performance deterioration after the accelerated durability test (1000 cycles, 1.3−1.7 V, 100 mV s^{-1}), whereas both Ir/C and Co_3O_4/C recorded a more than 30−40 mV increment of overpotential at 10 mA cm^{-2} under the identical test (Figures 6d, S19), manifesting the superior stability of the in situ-transformed catalyst. Moreover, continuous bulk electrolysis at a high current density (6 mA cm^{-2}) over 12 h was almost completely tolerable (Figure 6e): only a minute loss of current densities (∼10 mV enhancement of overpotential at 10 mA cm^2) was recorded after the bulk electrolysis. It should be mentioned that the nanoweb-like dispersed architectures are well-conserved during the long-term durability test (Figures 6f, S20), implying its structural stability. In a microscopic view, an adjacent phosphate group may stabilize the local structure of the catalyst against the repeating catalytic turnover.

The distinctive OER performances of the activated CoP can be explained by its inherent nature, which we have already discussed. Even though we could not get additional quantitative data related to the real active surface area, the porous and nanoweb-like dispersed morphologies can be favorable to render more accessible active sites, fast diffusion of reactants/products, and even rapid proton-coupled electron transfer (PCET).[2b,5e] For the OER process, several theoretical and experimental mechanistic studies suggested a one-electron, one-proton reaction (PCET) mechanism that involves Co(III)−OH and Co(IV)-O moieties, which are likely located within edge-sharing or vertex-sharing Co-oxo/hydroxo molecular units.[25] In fact, both molecular units are remarkable structural analogies to the Mn_3CaO_4 core of the OEC in photosystem II, along with almost identical metal−metal and metal−oxo distances (Figures 1a, 5d).[13h,25] As we confirmed, their EXAFS representations are quite consistent with the active state of the present catalyst; thus, improved OER kinetics and low-charge transfer resistance can be attributed to the enrichment of such molecular units within local structures. In addition, the presence of the phosphate species might be responsible for the effective OER kinetics. A surface phosphate group either in solution or surface-bound has been known to assist PCET during OER catalysis.[1,12,13] A synergetic effect between cobalt oxides and cobalt phosphate was also suggested.[5h] A more detailed mechanistic elucidation for the present system is now underway in our laboratory.

2.4. Cathodic Behaviors of CoP Nanoparticles: HER Performances. So far, we have focused on the anodic electrochemical nature of the present CoP nanoparticles. Finally, the cathodic behaviors of the as-prepared CoP/C were investigated, particularly for its alkaline HER performances (Figure 7). For HER catalysts, development of nonnoble metal (Mo, Ni, Co)-based heterogeneous catalysts has been actively pursued to replace expensive Pt-based materials.[26] Nevertheless, most of the recently developed HER catalysts, including metal phosphide systems with different nanostructures,[27] function well mainly in acid, whereas almost all the best OER catalysts operate well in basic (or neutral) media.[5,26,27]

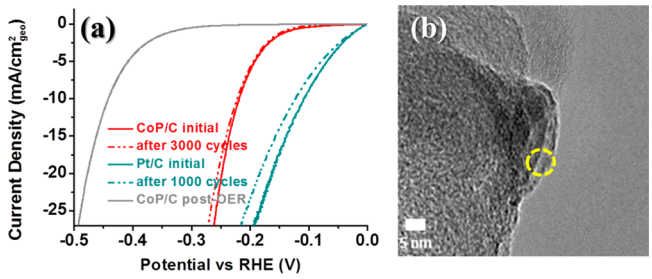

Figure 7. (a) HER polarization curves of original CoP/C, 20 wt % Pt/C, and post-OER state of CoP/C obtained at H_2 saturated 0.1 M KOH with a scan rate of 2 mV s^{-1} (catalyst loadings: 0.05 mg cm^{-2} for Co mass and 0.016 mg cm^{-2} for Pt mass). All given data is *iR*-compensated (R ∼ 30 ohm). (b) TEM image of CoP/C after HER durability test (0.05 ∼ −0.35 V, 100 mV s^{-1}, 3000 cycles). The preserved coating layer structures are marked with a yellow circle.

This discrepancy is one of the major issues currently hampering the water-splitting reaction. To our delight, the present CoP/C displayed efficient HER performance under alkaline conditions (0.1 M KOH), even with relatively low cobalt mass loading (∼0.05 mg cm^{-2}). It exhibits large cathodic current densities with a small onset potential (<100 mV) and achieved a current density of 20 mA cm^{-2} at an overpotential of 250 mV (Figure 7a). Pleasingly, the efficiency of the present catalyst is not only close to that of Pt/C but also favorably comparable to the best reported other cobalt-based alkaline HER catalysts, such as cobalt-embedded, nitrogen-rich carbon nanotubes (overpotential of 370 mV at 10 mA cm^{-2})[26i] and self-supported cobalt phosphide nanowires on carbon cloth (overpotential of 209 mV at 10 mA cm^{-2}).[27a] The present CoP/C also displays an efficient hydrogen-evolving nature, even in the acidic medium (0.5 M H_2SO_4) (Figure S21), achieving a current density of 10 mA/cm^2 at an overpotential of ∼130 mV. The performance is favorably comparable to the best reported nonprecious HER catalysts operating in acid (Table S1).

The catalyst exhibits outstanding durability in the alkaline medium. The initial HER performance was maintained almost perfectly, even after 3000 cycles (0.05 ∼ −0.35 V, 100 mV s^{-1}), but Pt/C experienced a noticeable performance degradation during 1000 cycles under identical conditions (Figure 7a). The morphology of the CoP nanoparticle and its coating layer structure were preserved (albeit it became thinner) even after the long-term stability test (Figures 7b, S22); thus, we suspect that the amorphous coating layers are somehow responsible for the efficient and durable HER performances. This aspect is especially noteworthy in view of the fact that such outer layer structures (Figure 3) have never been addressed in other metal phosphide-based HER catalysts. On the other hand, the post-OER state of CoP/C, which experienced anodic CV cycles (1.0−1.8 V, 5 mV s^{-1}, 2 cycles) in advance of the HER measurement, showed poor HER efficiency, highly inferior to the original as-prepared state of CoP/C (Figure 7a). The result indicates that the in situ transformed OER-active environments are not effective toward HER. Along with the versatile natures of the present CoP nanoparticles upon the applied potentials, we could represent efficient alkaline electrocatalytic systems for both HER and OER from one material.

3. CONCLUSION

In summary, we have described novel aspects of cobalt phosphide nanoparticles in alkaline water electrolysis, partic-

DOI: 10.1021/acscatal.5b00349
ACS Catal. 2015, 5, 4066−4074

ularly for the oxygen evolution reaction. Although the present CoP nanoparticles displayed efficient and durable alkaline hydrogen-evolving performances at cathodic potentials, they were revealed to experience dramatic metamorphosis under oxygen-evolution conditions, engendering dispersed morphologies and unique microscopic local environments that are highly effective toward OER. Not only excellent OER efficiency favorably comparable to a precious iridium catalyst, but also remarkable durability was achieved by the in situ-transformed catalyst. The present work highlights that control of restructuring behavior upon anodic potentials can be available in a nanoparticle system by design of its precursive state to be coupled with possible ligating species that would regulate the overall redox switching nature of cobalt.

■ ASSOCIATED CONTENT

Supporting Information

The Supporting Information is available free of charge on the ACS Publications website at DOI: 10.1021/acscatal.5b00349.

Details of synthesis and characterization method of present materials as well as additional electrochemical data (PDF)

■ AUTHOR INFORMATION

Corresponding Author

*E-mail: ysj@kist.re.kr.

Present Address

§N.J.: Graduate School of Energy Science and Technology (GEST), Chungnam National University, Daejeon 305-764, Republic of Korea

Notes

The authors declare no competing financial interest.

■ ACKNOWLEDGMENTS

This research was supported financially by Global Frontier R Program on Center for Multiscale Energy System (NRF-2012M3A6A7054283), the NRF grant funded by MSIP (2014R1A2A2A04003865), the KIST Institutional Program of Korea Institute of Science and Technology (KIST), the New and Renewable Energy Core Technology Program of KETEP grant funded by MOTIE (20133030011320), and the KCRC grant funded by MSIP (2014M1A8A1049349).

■ REFERENCES

(1) Cook, T. R.; Dogutan, D. K.; Reece, S. Y.; Surendranath, Y.; Teets, T. S.; Nocera, D. G. *Chem. Rev.* **2010**, *110*, 6474−6502.

(2) (a) Subbaraman, R.; Tripkovic, D.; Chang, K.-C.; Strmcnik, D.; Paulikas, A. P.; Hirunsit, P.; Chan, M.; Greeley, J.; Stamenkovic, V.; Markovic, N. M. *Nat. Mater.* **2012**, *11*, 550−557. (b) Mirzakulova, E.; Khatmullin, R.; Walpita, J.; Corrigan, T.; Vargas-Barbosa, N. M.; Vyas, S.; Oottikkal, S.; Manzer, S. F.; Hadad, C. M.; Glusac, K. D. *Nat. Chem.* **2012**, *4*, 794−801.

(3) (a) Hara, M.; Mallouk, T. E. *Chem. Commun.* **2000**, *19*, 1903−1904. (b) Hara, M.; Waraksa, C. C.; Lean, J. T.; Lewis, B. A.; Mallouk, T. E. *J. Phys. Chem. A* **2000**, *104*, 5275−5280. (c) Morris, N. D.; Suzuki, M.; Mallouk, T. E. *J. Phys. Chem. A* **2004**, *108*, 9115−9119.

(4) (a) Esswein, A. J.; McMurdo, M. J.; Ross, P. N.; Bell, A. T.; Tilley, T. D. *J. Phys. Chem. C* **2009**, *113*, 15068−15072. (b) Lu, B.; Cao, D.; Wang, P.; Wang, G.; Gao, Y. *Int. J. Hydrogen Energy* **2011**, *36*, 72−78. (c) Wee, T.-L.; Sherman, B. D.; Gust, D.; Moore, A. L.; Moore, T. A.; Liu, Y.; Scaiano, J. C. *J. Am. Chem. Soc.* **2011**, *133*, 16742−16745. (d) Rosen, J.; Hutchings, G. S.; Jiao, F. *J. Am. Chem. Soc.* **2013**, *135*, 4516−4521.

(5) (a) Suntivich, J.; May, K. J.; Gasteiger, H. A.; Goodenough, J. B.; Shao-Horn, Y. *Science* **2011**, *334*, 1383−1385. (b) Zanarini, S.; Vankova, S.; Hernandez, S.; Ijeri, V. S.; Armandi, M.; Garrone, E.; Bonelli, B.; Onida, B.; Spinelli, P. *Chem. Commun.* **2012**, *48*, 5754−5756. (c) Gao, M.-R.; Xu, Y.-F.; Jiang, J.; Zheng, Y.-R.; Yu, S.-H. *J. Am. Chem. Soc.* **2012**, *134*, 2930−2933. (d) Conrad, F.; Bauer, M.; Sheptyakov, D.; Weyeneth, S.; Jaeger, D.; Hametner, K.; Car, P.-E.; Patscheider, J.; Günther, D.; Patzke, G. R. *RSC Adv.* **2012**, *2*, 3076−3082. (e) Zou, X.; Goswami, A.; Asefa, T. *J. Am. Chem. Soc.* **2013**, *135*, 17242−17245. (f) Liu, Y.; Cheng, H.; Lyu, M.; Fan, S.; Liu, Q.; Zhang, W.; Zhi, Y.; Wang, C.; Xiao, C.; Wei, S.; Ye, B.; Xie, Y. *J. Am. Chem. Soc.* **2014**, *136*, 15670−15675. (g) Zheng, Y.-R.; Gao, M.-R.; Gao, Q.; Li, H.-H.; Xu, J.; Wu, Z.-Y.; Yu, S.-H. *Small* **2015**, *11*, 182−188. (h) Ahn, H. S.; Tilley, T. D. *Adv. Funct. Mater.* **2013**, *23*, 227−233.

(6) Yeo, B. S.; Bell, A. T. *J. Am. Chem. Soc.* **2011**, *133*, 5587−5593.

(7) (a) Liang, Y.; Li, Y.; Wang, H.; Zhou, J.; Wang, J.; Regier, T.; Dai, H. *Nat. Mater.* **2011**, *10*, 780−786. (b) Liang, Y.; Wang, H.; Zhou, J.; Li, Y.; Wang, J.; Regier, T.; Dai, H. *J. Am. Chem. Soc.* **2012**, *134*, 3517−3523. (c) Liang, Y.; Wang, H.; Diao, P.; Chang, W.; Hong, G.; Li, Y.; Gong, M.; Xie, L.; Zhou, J.; Wang, J.; Regier, T. Z.; Wei, F.; Dai, H. *J. Am. Chem. Soc.* **2012**, *134*, 15849−15857. (d) Gao, M.-R.; Cao, X.; Gao, Q.; Xu, Y.-F.; Zheng, Y.-R.; Jiang, J.; Yu, S.-H. *ACS Nano* **2014**, *8*, 3970−3978.

(8) Doyle, R. L.; Godwin, I. J.; Brandon, M. P.; Lyons, M. E. G. *Phys. Chem. Chem. Phys.* **2013**, *15*, 13737−13783.

(9) Lee, S. W.; Carlton, C.; Risch, M.; Surendranath, Y.; Chen, S.; Furutsuki, S.; Yamada, A.; Nocera, D. G.; Shao-Horn, Y. *J. Am. Chem. Soc.* **2012**, *134*, 16959−16962.

(10) McEvoy, J. P.; Brudvig, G. W. *Chem. Rev.* **2006**, *106*, 4455−4483.

(11) Symes, M. D.; Surendranath, Y.; Lutterman, D. A.; Nocera, D. G. *J. Am. Chem. Soc.* **2011**, *133*, 5174−5177.

(12) Yin, Q.; Tan, J. M.; Besson, C.; Geletii, Y. V.; Musaev, D. G.; Kuznetsov, A. E.; Luo, Z.; Hardcastle, K. I.; Hill, C. L. *Science* **2010**, *328*, 342−345.

(13) (a) Kanan, M. W.; Nocera, D. G. *Science* **2008**, *321*, 1072−1075. (b) Kanan, M. W.; Surendranath, Y.; Nocera, D. G. *Chem. Soc. Rev.* **2009**, *38*, 109−114. (c) Cobo, S.; Heidkamp, J.; Jacques, P.-A.; Fize, J.; Fourmond, V.; Guetaz, L.; Jousselme, B.; Ivanova, V.; Dau, H.; Palacin, S.; Fontecave, M.; Artero, V. *Nat. Mater.* **2012**, *11*, 802−807. (d) Steinmiller, E. M. P.; Choi, K.-S. *Proc. Natl. Acad. Sci. U. S. A.* **2009**, *106*, 20633−20636. (e) Risch, M.; Khare, V.; Zaharieva, I.; Gerencser, L.; Chernev, P.; Dau, H. *J. Am. Chem. Soc.* **2009**, *131*, 6936−6937. (f) Kanan, M. W.; Yano, J.; Surendranath, Y.; Dincă, M.; Yachandra, V. K.; Nocera, D. G. *J. Am. Chem. Soc.* **2010**, *132*, 13692−13701. (g) Hu, X. L.; Piccinin, S.; Laio, A.; Fabris, S. *ACS Nano* **2012**, *6*, 10497−10504. (h) Symes, M. D.; Surendranath, Y.; Lutterman, D. A.; Nocera, D. G. *J. Am. Chem. Soc.* **2011**, *133*, 5174−5177.

(14) (a) Park, J.; Koo, B.; Yoon, K. Y.; Hwang, Y.; Kang, M.; Park, J.-G.; Hyeon, T. *J. Am. Chem. Soc.* **2005**, *127*, 8433−8440. (b) Ha, D.-H.; Moreau, L. M.; Bealing, C. R.; Zhang, H.; Hennig, R. G.; Robinson, R. D. *J. Mater. Chem.* **2011**, *21*, 11498−11510. (c) Yang, D.; Zhu, J.; Rui, X.; Tan, H.; Cai, R.; Hoster, H. E.; Yu, D. Y. W.; Hng, H. H.; Yan, Q. *ACS Appl. Mater. Interfaces* **2013**, *5*, 1093−1099. (d) Zhang, H.; Ha, D.-H.; Hovden, R.; Kourkoutis, L. F.; Robinson, R. D. *Nano Lett.* **2011**, *11*, 188−197.

(15) Kim, H.; Chae, Y.; Lee, D. H.; Kim, M.; Huh, J.; Kim, Y.; Kim, H.; Kim, H. J.; Kim, S. O.; Baik, H.; Choi, K.; Kim, J. S.; Yi, G.-R.; Lee, K. *Angew. Chem., Int. Ed.* **2010**, *49*, 5712−5716.

(16) (a) Du, G.; Liu, X.; Zong, Y.; Hor, T. S. A.; Yuc, A.; Liu, Z. *Nanoscale* **2013**, *5*, 4657−4661. (b) Biesinger, M. C.; Payne, B. P.; Grosvenor, A. P.; Lau, L. W. M.; Gerson, A. R.; Smart, R. St. C. *Appl. Surf. Sci.* **2011**, *257*, 2717−2730. (c) Yang, J.; Liu, H.; Martens, W. N.; Frost, R. L. *J. Phys. Chem. C* **2010**, *114*, 111−119. (d) Wagner, C. D.; Naumkin, A. V.; Kraut-Vass, A.; Allison, J. W.; Powell, C. J.; Jr. Rumble, J. R. X-Ray Photoelectron Spectroscopy Database. *NIST Standard Reference Database 20, Version 4.1* (web version); http://srdata.nist.gov/xps, accessed 2012.

DOI: 10.1021/acscatal.5b00349
ACS Catal. 2015, 5, 4066−4074

(17) (a) Rotole, J. A.; Sherwood, P. M. A. *Chem. Mater.* **2001**, *13*, 3933−3942. (b) Brow, R. K.; Reidmeyer, M. R.; Day, D. E. *J. Non-Cryst. Solids* **1988**, *99*, 178−189.
(18) (a) Grosvenor, A. P.; Wik, S. D.; Cavell, R. G.; Mar, A. *Inorg. Chem.* **2005**, *44*, 8988−8998. (b) Abu, I. I.; Smith, K. J. *J. Catal.* **2006**, *241*, 356−366.
(19) (a) Kortányi, T. I. *Appl. Catal., A* **2003**, *239*, 253−267. (b) Kawashima, A.; Asami, K.; Hashimoto, K. *Corros. Sci.* **1984**, *24*, 807−823. (c) Siconolfi, D. J.; Frankenthal, R. P. *J. Electrochem. Soc.* **1989**, *136*, 2475−2480.
(20) (a) Lyons, M. E. G.; Brandon, M. P. *Int. J. Electrochem. Sci.* **2008**, *3*, 1386−1424. (b) Nakagawa, T.; Beasley, C. A.; Murray, R. W. *J. Phys. Chem. C* **2009**, *113*, 12958−12961. (c) Lyons, M. E. G.; Brandon, M. P. *J. Electroanal. Chem.* **2010**, *641*, 119−130. (d) He, Q.; Li, Q.; Khene, S.; Ren, X.; López-Suárez, F. E.; Lozano-Castelló, D.; Bueno-López, A.; Wu, G. *J. Phys. Chem. C* **2013**, *117*, 8697−8707.
(21) Lu, J.; Lei, Y.; Lau, K. C.; Luo, X.; Du, P.; Wen, J.; Assary, R. S.; Das, U.; Miller, D. J.; Elam, J. W.; Albishri, H. M.; El-Hady, D. A.; Sun, Y.-K.; Curtiss, L. A.; Amine, K. *Nat. Commun.* **2013**, *4*, 2383.
(22) Chou, N. H.; Ross, P. N.; Bell, A. T.; Tilley, T. D. *ChemSusChem* **2011**, *4*, 1566−1569.
(23) Bajdich, M.; García-Mota, M.; Vojvodic, A.; Nørskov, J. K.; Bell, A. T. *J. Am. Chem. Soc.* **2013**, *135*, 13521−13530.
(24) Matsumoto, Y.; Sato, E. *Mater. Chem. Phys.* **1986**, *14*, 397−426.
(25) (a) Surendranath, Y.; Kanan, M. W.; Nocera, D. G. *J. Am. Chem. Soc.* **2010**, *132*, 16501−16509. (b) Gerken, J. B.; McAlpin, J. G.; Chen, J. Y. C.; Rigsby, M. L.; Casey, W. H.; Britt, R. D.; Stahl, S. S. *J. Am. Chem. Soc.* **2011**, *133*, 14431−14442. (c) McAlpin, J. G.; Surendranath, Y.; Dinca, M.; Stich, T. A.; Stoian, S. A.; Casey, W. H.; Nocera, D. G.; Britt, R. D. *J. Am. Chem. Soc.* **2010**, *132*, 6882−6883.
(26) For the selected examples of Mo, Ni, Co-based HER catalysts, see: (a) Merki, D.; Hu, X. *Energy Environ. Sci.* **2011**, *4*, 3878−3888. (b) Kibsgaard, J.; Chen, Z.; Reinecke, B. N.; Jaramillo, T. F. *Nat. Mater.* **2012**, *11*, 963−969. (c) Vrubel, H.; Hu, X. *Angew. Chem., Int. Ed.* **2012**, *51*, 12703−12706. (d) Chen, W.-F.; Wang, C.-H.; Sasaki, K.; Marinkovic, N.; Xu, W.; Muckerman, J. T.; Zhu, Y.; Adzic, R. R. *Energy Environ. Sci.* **2013**, *6*, 943−951. (e) Kong, D.; Wang, H.; Cha, J. J.; Pasta, M.; Koski, K. J.; Yao, J.; Cui, Y. *Nano Lett.* **2013**, *13*, 1341−1347. (f) Chen, W.-F.; Sasaki, K.; Ma, C.; Frenkel, A. I.; Marinkovic, N.; Muckerman, J. T.; Zhu, Y.; Adzic, R. R. *Angew. Chem., Int. Ed.* **2012**, *51*, 6131−6135. (g) Kong, D.; Wang, H.; Lu, Z.; Cui, Y. *J. Am. Chem. Soc.* **2014**, *136*, 4897−4900. (h) Xu, Y.-F.; Gao, M.-R.; Zheng, Y.-R.; Jiang, J.; Yu, S.-H. *Angew. Chem., Int. Ed.* **2013**, *52*, 8546−8550. (i) Zou, X.; Huang, X.; Goswami, A.; Silva, R.; Sathe, B. R.; Mikmeková, E.; Asefa, T. *Angew. Chem., Int. Ed.* **2014**, *53*, 4372−4376. (j) Jaramillo, T. F.; Jørgensen, K. P.; Bonde, J.; Nielsen, J. H.; Horch, S.; Chorkendorff, I. *Science* **2007**, *317*, 100−102. (k) Li, Y.; Wang, H.; Xie, L.; Liang, Y.; Hong, G.; Dai, H. *J. Am. Chem. Soc.* **2011**, *133*, 7296−7299. (l) Cao, B.; Veith, G. M.; Neuefeind, J. C.; Adzic, R. R.; Khalifah, P. G. *J. Am. Chem. Soc.* **2013**, *135*, 19186−19192. (m) Tian, J.; Liu, Q.; Cheng, N.; Asiri, A. M.; Sun, X. *Angew. Chem., Int. Ed.* **2014**, *53*, 9577−9581.
(27) For the examples of metal phosphide HER catalysts, see: (a) Tian, J.; Liu, Q.; Asiri, A. M.; Sun, X. *J. Am. Chem. Soc.* **2014**, *136*, 7587−7590. (b) Liu, Q.; Tian, J.; Cui, W.; Jiang, P.; Cheng, N.; Asiri, A. M.; Sun, X. *Angew. Chem., Int. Ed.* **2014**, *53*, 6710−6714. (c) Popczun, E. J.; Read, C. G.; Roske, C. W.; Lewis, N. S.; Schaak, R. E. *Angew. Chem., Int. Ed.* **2014**, *53*, 5427−5430. (d) Popczun, E. J.; McKone, J. R.; Read, C. G.; Biacchi, A. J.; Wiltrout, A. M.; Lewis, N. S.; Schaak, R. E. *J. Am. Chem. Soc.* **2013**, *135*, 9267−9270. (e) Feng, L.; Vrubel, H.; Bensimon, M.; Hu, X. *Phys. Chem. Chem. Phys.* **2014**, *16*, 5917−5921. (f) Xiao, P.; Sk, M. A.; Thia, L.; Ge, X.; Lim, R. J.; Wang, J.-Y.; Lim, K. H.; Wang, X. *Energy Environ. Sci.* **2014**, *7*, 2624−2629.

DOI: 10.1021/acscatal.5b00349
ACS Catal. 2015, 5, 4066−4074